J. Fluid Mech. (1997), *vol.* 351, *pp.* 119–138. Printed in the United Kingdom

© 1997 Cambridge University Press

The generation of internal waves by vibrating elliptic cylinders. Part 2. Approximate viscous solution

By D. G. HURLEY AND G. KEADY
Mathematics Department, University of Western Australia, Nedlands, WA 6009, Australia

(Received 4 January 1996 and in revised form 16 June 1997)

An approximate theory is given for the generation of internal gravity waves in a viscous Boussinesq fluid by the rectilinear vibrations of an elliptic cylinder. A parameter λ which is proportional to the square of the ratio of the thickness of the oscillatory boundary layer that surrounds the cylinder to a typical dimension of its cross-section is introduced. When $\lambda \ll 1$ (or equivalently when the Reynolds number $R \gg 1$), the viscous boundary condition at the surface of the cylinder may to first order in λ be replaced by the inviscid one. A viscous solution is proposed for the case $\lambda \ll 1$ in which the Fourier representation of the stream function found in Part 1 (Hurley 1997) is modified by including in the integrands a factor to account for viscous dissipation. In the limit $\lambda \to 0$ the proposed solution becomes the inviscid one at each point in the flow field.

For ease of presentation the case of a circular cylinder of radius a is considered first and we take a to be the typical dimension of its cross-section in the definition of λ above. The accuracy of the proposed approximate solution is investigated both analytically and numerically and it is concluded that it is accurate throughout the flow field if λ is sufficiently small, except in a small region near where the characteristics touch the cylinder where viscous effects dominate.

Computations indicate that the velocity on the centreline on a typical beam of waves, at a distance s along the beam from the centre of the cylinder, agrees, within about 1 %, with the (constant) inviscid values provided $\lambda s/a$ is less than about 10^{-3}. This result is interpreted as indicating that those viscous effects which originate from the characteristics that touch the cylinder (places where the inviscid velocity is singular) reach the centreline of the beam when $\lambda s/a$ is about 10^{-3}. For larger values of s, viscous effects are significant throughout the beam and the velocity profile of the beam changes until it attains, within about 1 % when $\lambda s/a$ is about 2, the value given by the similarity solution obtained by Thomas & Stevenson (1972). For larger values of $\lambda s/a$, their similarity solution applies.

In an important paper Makarov *et al.* (1990) give an approximate solution for the circular cylinder that is very similar to ours. However, it does not reduce to the inviscid one when the viscosity is taken to be zero.

Finally it is shown that our results for a circular cylinder apply, after small modifications, to all elliptical cylinders.

1. Introduction

The inviscid theory described in Part 1, Hurley (1997), has two features that limit its applicability to a real fluid of small viscosity. First, the fluid velocities have inverse

https://doi.org/10.1017/S0022112097007039 Published online by Cambridge University Press

square-root singularities at all points of the characteristics that touch the vibrating cylinder, so that the kinetic energy of the fluid per unit length of characteristic is infinite. Also, the fluid velocities do not decay with increasing distance from the cylinder.

In the present paper we investigate how these two defects are alleviated if the fluid is assumed to be viscous while remaining with a linearized treatment. The basic equations are given in §2. In §3 we propose an approximate solution to the viscous flow, for the case when the Reynolds number R, defined in §2.1, is large. Specifically, the Fourier decompositions of the stream function of the inviscid solution, obtained in Part 1, are modified by including in the integrands factors to account for viscous dissipation. The proposed approximate solution applies to all elliptic cylinders but for ease of presentation it is described in §3 for the case of a circular cylinder. Section 4 gives extensive numerical results and in §5 our results are compared with both theoretical and experimental ones obtained by other investigations. Finally in §6 it is pointed out that the main properties of the flow for a circular cylinder also hold for all elliptic cylinders.

2. Basic equations

The problem is the same as that considered in Part 1, except that the stratified fluid of constant Brunt–Väisälä frequency N surrounding the elliptical cylinder is now supposed to be viscous of kinematic viscosity ν. As in Part 1, the ellipse has semi-axes a and b, the former being inclined at an angle θ to the horizontal. We introduce Cartesian axes, the x-axis being horizontal and the y-axis vertically up, and the origin of the coordinate system is at the centre of the cylinder. We suppose that the velocity of each point of the surface of the cylinder is $(U, V)\exp(-\mathrm{i}\omega t)$ where t is the time, and ω the angular frequency. The fluid motions may be described in terms of a stream function $\psi(x, y)\exp(-\mathrm{i}\omega t)$ such that the velocity (u, v) is

$$u = -\frac{\partial \psi}{\partial y}\mathrm{e}^{-\mathrm{i}\omega t}, \quad v = \frac{\partial \psi}{\partial x}\mathrm{e}^{-\mathrm{i}\omega t}, \tag{2.1}$$

and ψ satisfies

$$\eta^2 \frac{\partial^2 \psi}{\partial x^2} - \frac{\partial^2 \psi}{\partial y^2} + \frac{\mathrm{i}\nu}{\omega}\nabla^4 \psi = 0, \tag{2.2}$$

where

$$\eta^2 = N^2/\omega^2 - 1. \tag{2.3}$$

In addition, the velocities must vanish as (x, y) tends to infinity. The boundary condition on the cylinder is discussed in §2.1 below.

We introduce the coordinates

$$\sigma_+ = x\sin(\mu) - y\cos(\mu), \quad s_+ = x\cos(\mu) + y\sin(\mu), \tag{2.4}$$

where $0 < \mu < \pi/2$ and

$$0 < \eta = \cot(\mu). \tag{2.5}$$

In terms of them, (2.2) is

$$\frac{\partial^2 \psi}{\partial \sigma_+ \partial s_+} + \cot(2\mu)\frac{\partial^2 \psi}{\partial s_+^2} + \frac{\mathrm{i}\nu}{2\omega\eta}\left(\frac{\partial^2 \psi}{\partial \sigma_+^4} + 2\frac{\partial^4 \psi}{\partial \sigma_+^2 \partial s_+^2} + \frac{\partial^4 \psi}{\partial s_+^4}\right) = 0. \tag{2.6}$$

We also introduce the coordinates

$$\sigma_- = x\sin(\mu) + y\cos(\mu), \quad s_- = -x\cos(\mu) + y\sin(\mu). \tag{2.7}$$

https://doi.org/10.1017/S0022112097007039 Published online by Cambridge University Press

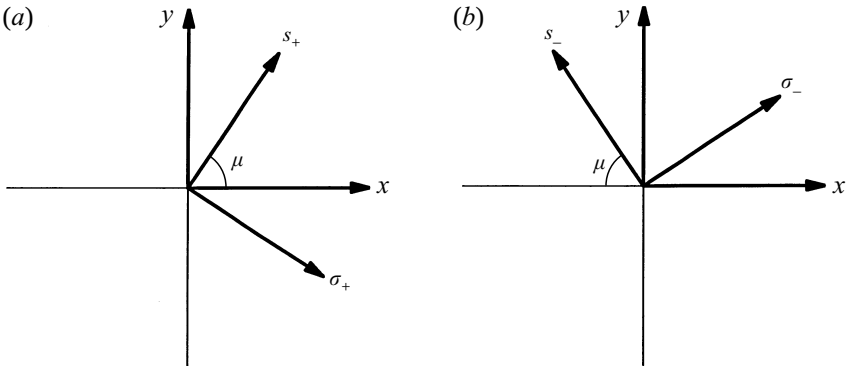


FIGURE 1. Notation. (*a*) $O\sigma_+ s_+$ axes, (*b*) $O\sigma_- s_-$ axes.

In terms of these, (2.2) is

$$\frac{\partial^2\psi}{\partial\sigma_-\,\partial s_-}-\cot(2\mu)\frac{\partial^2\psi}{\partial s_-^2}-\frac{\mathrm{i}\nu}{2\omega\eta}\left(\frac{\partial^4\psi}{\partial\sigma_-^4}+2\frac{\partial^4\psi}{\partial\sigma_-^2\,\partial s_-^2}+\frac{\partial^4\psi}{\partial s_-^4}\right)=0. \tag{2.8}$$

Figure 1 gives the directions of the $O\sigma_+ s_+$ and the $O\sigma_- s_-$ axes.

We now follow Thomas & Stevenson (1972) in introducing their 'boundary-layer approximation' by assuming that, in (2.6), derivatives with respect to σ_+ are much larger than those with respect to s_+. With this assumption, the equation is approximated by

$$\frac{\partial^2\psi}{\partial\sigma_+\,\partial s_+}+\frac{\mathrm{i}\nu}{2\omega\eta}\left(\frac{\partial^4\psi}{\partial\sigma_+^4}\right)=0. \tag{2.9}$$

Similarly, (2.8) is approximated by

$$\frac{\partial^2\psi}{\partial\sigma_-\,\partial s_-}-\frac{\mathrm{i}\nu}{2\omega\eta}\left(\frac{\partial^4\psi}{\partial\sigma_-^4}\right)=0. \tag{2.10}$$

2.1. *The boundary condition on the cylinder*

The vibrating cylinder will be surrounded by an oscillatory boundary layer whose thickness is order δ, where

$$\delta=(\nu/\omega)^{1/2}, \tag{2.11}$$

see Rosenhead (1963, p. 383) and Batchelor (1967, §5.13, p. 354).

We define

$$\lambda=\nu/(2c^2\omega\eta) \tag{2.12}$$

$$=1/(2\eta R), \tag{2.13}$$

where c is a typical dimension of the ellipse and

$$R=c^2\omega/\nu \tag{2.14}$$

is the Reynolds number.

Equations (2.11) and (2.12) show that an alternative expression for λ is

$$\lambda=\frac{1}{2\eta}\left(\frac{\delta}{c}\right)^2. \tag{2.15}$$

We suppose that $\lambda\ll 1$ or equivalently by (2.13) that $R\gg 1$. Then to first order in λ

https://doi.org/10.1017/S0022112097007039 Published online by Cambridge University Press

(Rosenhead 1963) the viscous no-slip boundary condition at the surface of the ellipse may be replaced by the inviscid one which is

$$\psi = Vx - Uy. \tag{2.16}$$

We also suppose that

$$U/(\omega c) \ll 1 \quad \text{and} \quad V/(\omega c) \ll 1, \tag{2.17}$$

because these must be satisfied for the present analysis, which is based on the 'acoustic limit', to be valid (Bell 1975).

3. Approximate viscous solution

It is convenient to consider the case of the circular cylinder first. We take its radius a as its typical dimension so that the parameter λ introduced in §2.1 above becomes

$$\lambda = \nu/(2a^2\omega\eta). \tag{3.1}$$

The proposed solution is

$$\psi = \psi_+(\sigma_+, s_+) + \psi_-(\sigma_-, s_-), \tag{3.2}$$

where

$$\psi_+ = \mp \mathrm{i}\alpha_+ a \int_0^\infty \frac{J_1(K)}{K} \exp\left(\mp K^3\lambda \frac{s_+}{a} \pm \mathrm{i}K\frac{\sigma_+}{a}\right) \mathrm{d}K, \quad \pm s_+ > 0, \tag{3.3}$$

$$\psi_- = \pm \mathrm{i}\alpha_- a \int_0^\infty \frac{J_1(K)}{K} \exp\left(\mp K^3\lambda \frac{s_-}{a} \mp \mathrm{i}K\frac{\sigma_-}{a}\right) \mathrm{d}K, \quad \pm s_- > 0, \tag{3.4}$$

and α_+ and α_- take the values given by (3.26) and (3.27) of Part 1: namely

$$\alpha_+ = \tfrac{1}{2}(V\sin(\mu) + U\cos(\mu) + \mathrm{i}[V\cos(\mu) - U\sin(\mu)]), \tag{3.5}$$

$$\alpha_- = \tfrac{1}{2}(V\sin(\mu) - U\cos(\mu) + \mathrm{i}[V\cos(\mu) + U\sin(\mu)]). \tag{3.6}$$

We focus attention on the beam of waves in the first quadrant for which

$$\psi_+ = -\mathrm{i}\alpha_+ a \int_0^\infty \frac{J_1(K)}{K} \exp\left(-K^3\lambda \frac{s_+}{a} + \mathrm{i}K\frac{\sigma_+}{a}\right) \mathrm{d}K, \quad s_+ > 0. \tag{3.7}$$

We note that at any point (σ_+, s_+) the limit as $\nu \to 0$ of ψ_+ given by (3.7) is that given by (3.31) of Part 1, the inviscid solution. The decay factor $\exp(-K^3\lambda s_+/a)$ in the integrand of (3.7) is the same as that used in Townsend (1966), Lighthill (1978) and Makarov, Neklyudov & Chasheckin (1990).

We also note that ψ_+ and ψ_- given by (3.3) and (3.4) satisfy (2.9) and (2.10) respectively which were obtained from the exact equations (2.6) and (2.8) by applying the boundary-layer approximation. In Appendices A and B we give derivations of (3.3) and (3.4) from the exact equations and conclude that if $\lambda \ll 1$ they provide a good approximation almost everywhere throughout the flow field. Their accuracy is also investigated numerically in §4.4 below.

3.1. *The smoothness of our solution*

It is important to investigate the smoothness of the solution given by (3.3) on the two rays $s_+ = 0$, $|\sigma_+| > a$, for if it were not smooth on them there would be singularities in its flow field.

As s_+ tends to ± 0, ψ_+ given by (3.3) attains the limiting values given by (3.35)–(3.37) of Part 1. Hence ψ_+ is continuous on $s_+ = 0$, $|\sigma_+| > a$ and so too will be all its derivatives with respect to σ_+. (We remark though that formal differentiation of the integral representations of ψ_+ with respect to σ_+, and then setting $s_+ = 0$ leads to

https://doi.org/10.1017/S0022112097007039 Published online by Cambridge University Press

divergent integrals). Also ψ_+ given by (3.3) satisfies (2.9) which may be integrated once to give (noting that the various derivatives of ψ_+ tend to zero as σ_+ tends to plus or minus infinity)

$$\frac{\partial \psi_+}{\partial s_+} + \mathrm{i}\lambda a^2 \frac{\partial^3 \psi_+}{\partial \sigma_+^3} = 0, \tag{3.8}$$

which shows that the first derivative of ψ_+ with respect to s_+ is continuous across $s_+ = 0$, $|\sigma_+| > a$. Higher derivatives with respect to s_+, and cross-derivatives are then handled similarly.

We conclude that ψ_+ given by (3.3) is infinitely differentiable with respect to both variables everywhere in the plane except on the line segment $s_+ = 0$ within the circle. A similar result holds for ψ_-.

3.2. *Further consideration of the boundary condition on the cylinder*

We note that in the inviscid solution given by (3.42) of Part 1, ψ_+ is independent of s_+. We denote this value by ψ_+^i. Now in our proposed solution given by (3.7), ψ_+ is a continuous function of $\lambda s_+/a$ up to the line $s_+ = 0$ on which it equals ψ_+^i. Hence $|\psi_+ - \psi_+^i|$ can be made arbitrarily small provided $\lambda s_+/a < \delta$ for some δ. Now the equation of the cylinder in the first quadrant is $s_+/a = (1 - \sigma_+^2/a^2)^{1/2}$. Hence, since $(1 - \sigma_+^2/a^2)^{1/2}$ is bounded, the inequality $\lambda s_+/a < \delta$ can be satisfied if λ is sufficiently small. We therefore conclude that on the surface of the cylinder ψ_+ differs from ψ_+^i by an amount that tends to zero with λ. A similar argument applies to ψ_+ on $s_+ < 0$ and to ψ_- on $s_- < 0$ and $s_- > 0$.

Hence our solution will satisfy the inviscid boundary condition (2.16) and hence, by the remarks in §2.1, the viscous one to leading order in λ with arbitrarily small relative error if λ is sufficiently small.

4. Numerical results

To save repeated writing of the long expressions in equations like (3.3) and (3.4) and similar formulae for their derivatives, we define functions I_e and I_o as follows:

$$I_e(n; w, d) = \int_0^\infty K^n J_1(K) \exp(-dK^3) \cos(wK)\, \mathrm{d}K, \tag{4.1}$$

$$I_0(n; w, d) = \int_0^\infty K^n J_1(K) \exp(-dK^3) \sin(wK)\, \mathrm{d}K, \tag{4.2}$$

where

$$d = \lambda s_+/a \quad \text{and} \quad w = \sigma_+/a. \tag{4.3}$$

4.1. *The velocity profiles in the beams and beam width*

Equations (3.7) and (4.1)–(4.3) show that for the beam of waves in the first quadrant

$$\psi_+ = -\mathrm{i}\alpha_+ a[I_e(-1; w, d) + \mathrm{i}I_o(-1; w, d)]. \tag{4.4}$$

The velocity components obtained by differentiation of this equation are

$$\frac{\partial \psi_+}{\partial \sigma_+} = \alpha_+[I_e(0; w, d) + \mathrm{i}I_o(0; w, d)], \tag{4.5}$$

$$\frac{\partial \psi_+}{\partial s_+} = \mathrm{i}\alpha_+ \lambda[I_e(2; w, d) + \mathrm{i}I_o(2; w, d)]. \tag{4.6}$$

The resulting profiles of the waves will be expressed in two ways.

First, we give values of the real and imaginary parts of $(1/\alpha_+)(\partial \psi_+/\partial \sigma_+)$, i.e. values of $I_e(0; w, d)$ and $I_o(0; w, d)$ respectively. These are given in figure 2 for various values

https://doi.org/10.1017/S0022112097007039 Published online by Cambridge University Press

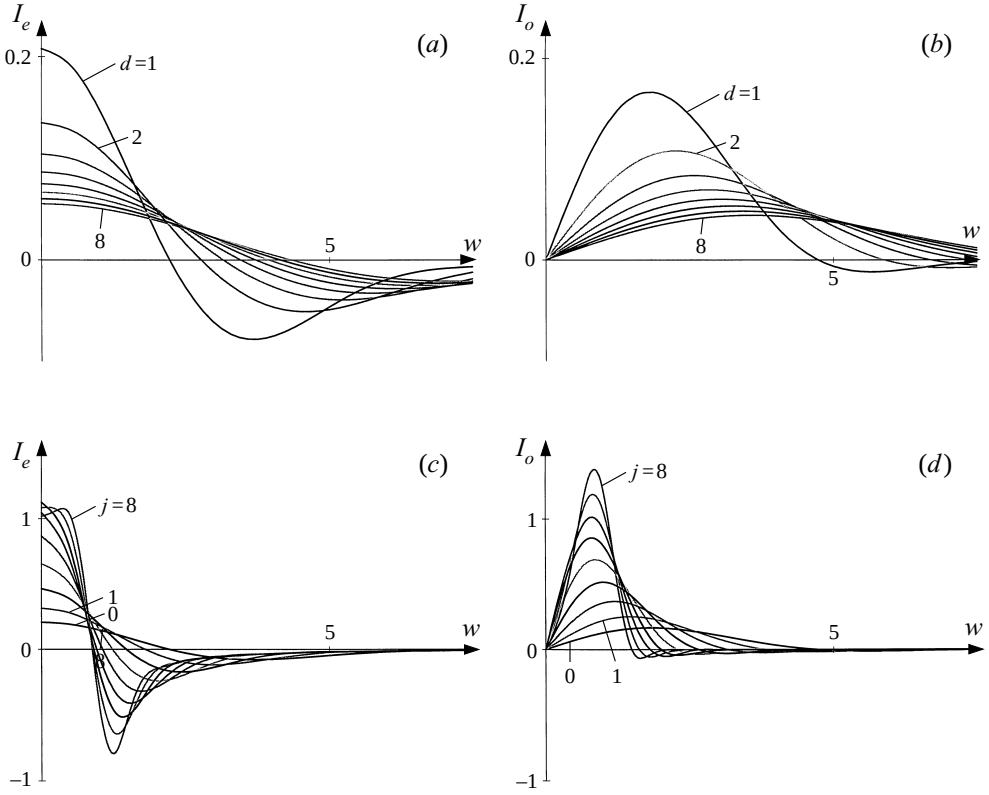


FIGURE 2. The I_e and I_o functions defining the velocity component $\partial\psi_+/\partial\sigma_+$ in the beams. (*a*) $I_e(0; w, d)$ and (*b*) $I_o(0; w, d)$, integer d from 1 to 8. (*c*) $I_e(0; w, d)$, $d = 2^{-j}$ and (*d*) $I_o(0; w, d)$, $d = 2^{-j}j$ from 0 to 8.

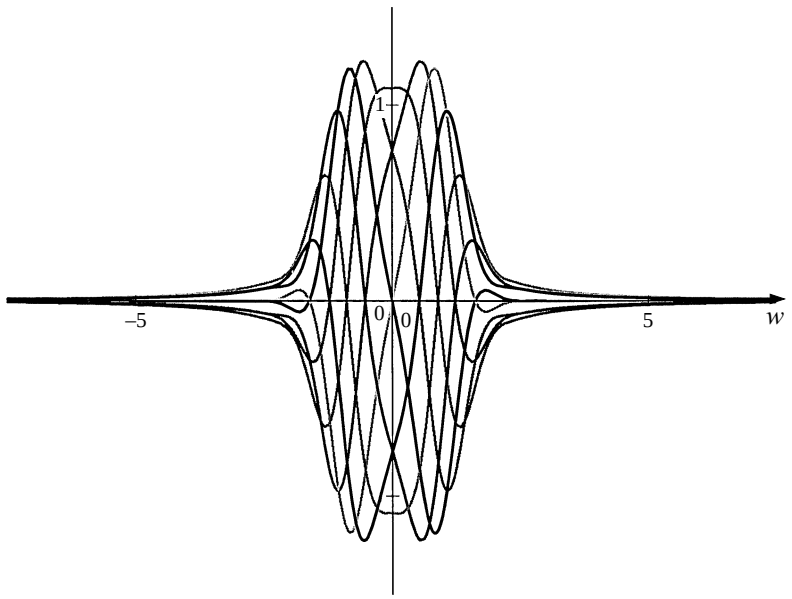


FIGURE 3. Wave forms $Re(\partial\psi_+/\partial\sigma_+)\exp(-i\omega t))$ at successive instants of time for a circular cylinder executing horizontal oscillations. $d = 2^{-7}$, $\omega t = \frac{1}{8}k\pi$, $k = 0, 1, 2, \ldots, 7$.

https://doi.org/10.1017/S0022112097007039 Published online by Cambridge University Press

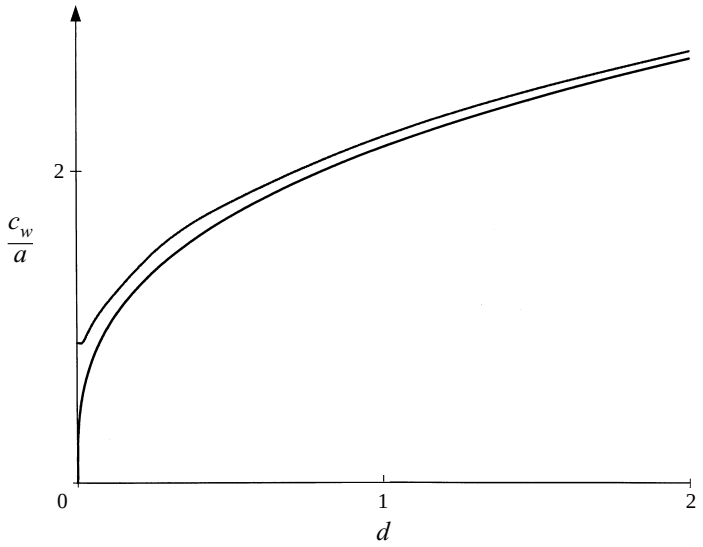


FIGURE 4. The beam width: upper curve for the finite cylinder, lower curve the far-field similarity solution (equation (4.8)).

of d, the smallest being $1/256$. The values of the inviscid solutions are plotted in Part 1, figure 4, and we see that the viscous profiles approach the inviscid ones, albeit rather slowly, as d tends to zero.

In the second method of presentation figure 3 gives, for the case $V = 0$, the velocity profiles, $\mathrm{Re}((\partial\psi_+/\partial\sigma_+)\exp(-\mathrm{i}\omega t))$ at successive instants of time. In particular, the velocity profiles for $d < 128$ are bimodal, in that the envelope of the curves has two maxima (Makarov *et al.* 1990).

Another quantity related to the velocity is the width of the beam. We define the width of the beam to be $2c_w$ where c_w satisfies $I_e(0; c_w/a, d) = 0$. Approximate values for the zero c_w/a can be read from figure 2. More accurate values can be obtained by numerically solving for the zero c_w/a from (4.1). These values of c_w/a are compared in figure 4 with the asymptotics, at large d, given by (4.8) below.

For d small, the beam width falls below 1, its minimum being about 0.9. Decreasing d further to really tiny values results in the beam width increasing, presumably tending to 1 as $d \to 0+$.

4.2. *Solution at large distances from the cylinder*

For large values of d, the major contribution to the integrals in (3.3) comes from small values of K so that we may replace $J_1(K)$ therein by $\frac{1}{2}K$. Thus, for example,

$$\frac{\partial\psi_+}{\partial\sigma_+} \sim \frac{\alpha_+}{2}\int_0^\infty K\exp(-K^3 d + \mathrm{i}wK)\,\mathrm{d}K, \quad d \to \infty, \tag{4.7}$$

where d and w are defined in (4.3). We recognize (4.7) as the solution obtained by Thomas & Stevenson (1972): see also Lighthill (1978, equation (343)). More generally, we have

$$2I_e(n; w, d) \sim \int_0^\infty K^{n+1}\exp(-dK^3)\cos(wK)\,\mathrm{d}K = d^{-(n+2)/3}c_n(wd^{-1/3}),$$

$$2I_o(n; w, d) \sim \int_0^\infty K^{n+1}\exp(-dK^3)\sin(wK)\,\mathrm{d}K = d^{-(n+2)/3}s_n(wd^{-1/3}).$$

https://doi.org/10.1017/S0022112097007039 Published online by Cambridge University Press

The notation c_n and s_n is that used in Thomas & Stevenson (1972). We remark that functions c_n and s_n can be written in closed forms, in terms of generalized hypergeometric functions (see Hurley & Keady 1996). The same functions occur in the singular solution of Makarov *et al.* (1990).

Profiles given by (4.7) are given in Thomas & Stevenson (1972), figures 2 and 3. It is clear that the results from our computations using (3.3) at larger d, as shown in our figures 2 and 3 herein, are similar. Detailed checks are given in Hurley & Keady (1996).

It is also possible to derive asymptotics for the beam width c_w for large values of d. We find

$$c_w/a \sim 2.15323 d^{1/3}, \quad d \gg 1. \tag{4.8}$$

Higher approximations are given in Hurley & Keady (1996).

4.3. *The solution on the centreline of the beam*

For $w = 0$, $I_o(n;0,d) = 0$ and *Mathematica 2.2* is able to evaluate the $I_e(n;0,d)$ integrals of (4.1) explicitly in terms of generalized hypergeometric functions. Here is its result for the integral – from just one obvious line of *Mathematica* – associated with the centreline velocity:

$$I_e(0;0,d) = 1 - {}_pF_q\left(\{\tfrac{1}{2}\}, \{\tfrac{1}{3}, \tfrac{1}{3}, \tfrac{2}{3}, \tfrac{2}{3}\}, \frac{-1}{11664 d^2}\right) + \frac{\Gamma(\frac{2}{3})\,{}_pF_q\left(\{\tfrac{5}{6}\}, \{\tfrac{2}{3}, \tfrac{2}{3}, 1, \tfrac{4}{3}\}, \frac{-1}{11664 d^2}\right)}{6 d^{2/3}} - \frac{\Gamma(\tfrac{4}{3})\,{}_pF_q\left(\{\tfrac{7}{6}\}, \{1, \tfrac{4}{3}, \tfrac{4}{3}, \tfrac{5}{3}\}, \frac{-1}{11664 d^2}\right)}{48 d^{4/3}}.$$

We have checked *Mathematica*'s numerical results against independent numerical evaluations of the integral. The closed form facilitates evaluation of $I_e(0;0,d)$ at much smaller values of d than was practical for general values of w. As regards asymptotic analyses, *Mathematica*'s representation is still better for the case d large, and, at least at version *2.2*, it does not seem straightforward to extract asymptotics for d small. Nevertheless, its numeric capabilities with these special functions is good into values where d is small.

Values of $I_e(0;0,d)$, which, by (4.5) is $1/\alpha_+$ times the centreline velocity, are compared in figure 5(*a*) with the asymptotic values given by (4.7) which are

$$I_e(0;0,d) \sim \tfrac{1}{6}\Gamma(\tfrac{2}{3})\, d^{-2/3} \doteq 0.226 d^{-2/3}, \quad d \gg 1. \tag{4.9}$$

The figure shows that the similarity solution is a good approximation for $d > 2$.

We now discuss the results for small values of d, where we expect the inviscid theory to hold. In this theory, each quantity is independent of s_+. We therefore expect ψ_+, $\partial\psi_+/\partial\sigma_+$ and $\partial\psi_+/\partial s_+$ to tend to appropriate values, independent of d, for d small.

For $d = 0$ and $w = 0$, equation (4.4) gives

$$\psi_+ = -\mathrm{i}\alpha_+ a I_e(-1;0,0) = -\mathrm{i}\alpha_+ a,$$

the latter by consideration of the inviscid ψ_+. Hence we expect

$$I_e(-1;0,d) \to 1 \quad \text{as} \quad d \to 0. \tag{4.10}$$

The other limiting behaviours may similarly be shown to be

$$I_e(0;0,d) \to 1 \quad \text{as} \quad d \to 0, \tag{4.11}$$

and

$$I_e(2;0,d) \to 0 \quad \text{as} \quad d \to 0. \tag{4.12}$$

https://doi.org/10.1017/S0022112097007039 Published online by Cambridge University Press

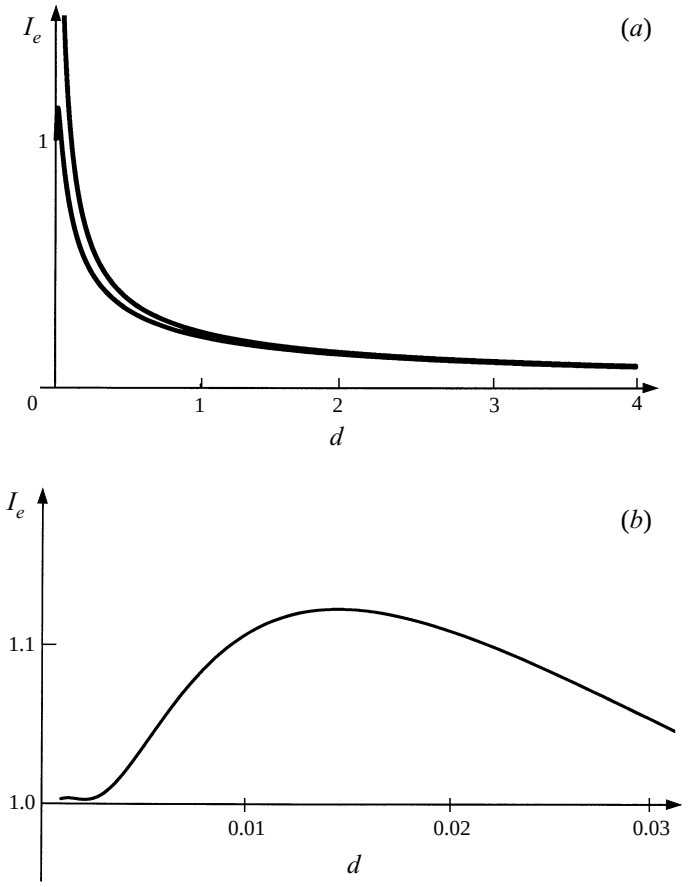


FIGURE 5. $I_e(0;0,d)$ (*a*) for large d and its asymptotics; (*b*) for small d.

Some indication of the limit (4.11) is evident at the left-hand end of figure 5(*a*). However, the behaviour at small d is rather non-uniform. The overshoot to just beyond 1, before falling back, is evident in the figure. Figure 5(*b*) plots $I_e(0;0,d)$ at small values of d. (Computations for other values of n, with particular attention to small values of d, are reported in detail in Hurley & Keady 1996.) The computations accord with the limits above and show that (4.10) and (4.11) are within 1% of being attained if $d < 10^{-3}$.

The results discussed earlier in this section suggest that it is convenient to split the range $0 < d < \infty$ into three sub-ranges as follows.

Region I is the range $0 < d < 10^{-3}$. At $d = 0$ the profile is the inviscid one and, as d is increased, viscous effects extend inwards from $w = \pm 1$ and reach the centreline after about $d = 10^{-3}$. The velocity profile across the beam is 'bimodal', being just a smoothed version of the inviscid one. (For definition of 'bimodal' and 'unimodal' see Makarov *et al.* 1990.)

Region II is the range $10^{-3} < d < 2$. Viscous effects are important throughout the beam and the velocity profile changes as d is increased, starting 'bimodal' and becoming 'unimodal', and becoming very close to the similarity profile at about $d = 2$.

Region III is the range $d > 2$ and the similarity solution applies everywhere there. The velocity profile is 'unimodal'.

https://doi.org/10.1017/S0022112097007039 Published online by Cambridge University Press

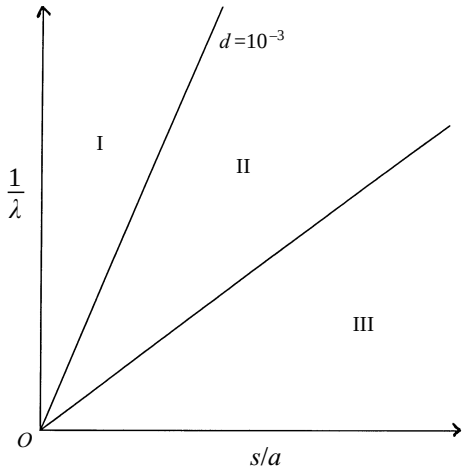


FIGURE 6. Schematic diagram of regions I, II and III of the $(s_+/a, 1/\lambda)$-plane.

In figure 6 we have sketched regions I, II and III.

A different split involves s_+.

In the region $|s_+| \leqslant a$ the ψ_+ and ψ_- beams overlap.

In the region $|s_+| > 3a$, for all practical purposes when λ is small, the ψ_- solution can be ignored within the region defined by the ψ_+ beam.

4.4. *Validity of our boundary-layer approximation*

As we pointed out in §3 expressions (3.3) and (3.4) for ψ_+ and ψ_- satisfy (2.9) and (2.10) respectively that were derived from the exact equations (2.6) and (2.8) by introducing the 'boundary-layer approximation'. For ψ_+ this approximation assumes that its derivatives with respect to σ_+ are much larger than its derivatives with respect to s_+. We now investigate the validity of this assumption.

We will assume that it is satisfied in regions where

$$\left|\frac{\partial \psi_+}{\partial s_+}\right| \ll \left|\frac{\partial \psi_+}{\partial \sigma_+}\right|. \tag{4.13}$$

Now, integration of (2.9) with respect to σ_+ gives

$$\frac{\partial \psi_+}{\partial s_+} + \frac{\mathrm{i}\nu}{2\omega\eta}\left(\frac{\partial^3 \psi_+}{\partial \sigma_+^3}\right) = f(s_+), \tag{4.14}$$

and $f(s_+)$ must vanish since both terms on the left-hand side of (4.14) tend to zero as σ_+ tends to plus or minus infinity. Hence

$$\frac{\partial \psi_+}{\partial s_+} + \frac{\mathrm{i}\nu}{2\omega\eta}\left(\frac{\partial^3 \psi_+}{\partial \sigma_+^3}\right) = 0. \tag{4.15}$$

Hence, in terms of w defined in (4.3), the condition (4.13) can be written

$$\lambda \left|\frac{\partial^3 \psi_+}{\partial w^3}\right| \ll \left|\frac{\partial \psi_+}{\partial w}\right|. \tag{4.16}$$

In discussing this condition, we consider the regions I, II and III of the $(s_+/a, 1/\lambda)$-plane that were defined before and are shown schematically in figure 6.

https://doi.org/10.1017/S0022112097007039 Published online by Cambridge University Press

In region III, the similarity solution holds, so that ψ_+ is given by

$$\psi_+ = -\mathrm{i}\frac{\alpha_+ a}{2d^{1/3}}\int_0^\infty \exp(-k^3+\mathrm{i}k\zeta)\,\mathrm{d}k = -\mathrm{i}\frac{\alpha_+ a}{2d^{1/3}}e_0(\zeta), \tag{4.17}$$

where

$$\zeta = \frac{\sigma_+/a}{(\lambda s_+/a)^{1/3}} = \frac{w}{d^{1/3}} \tag{4.18}$$

is the similarity parameter, and $e_0(\zeta)$ is a function of ζ.

Equation (4.7) etc. then gives

$$r = \frac{|\partial\psi_+/\partial s_+|}{|\partial\psi_+/\partial\sigma_+|} = \frac{\lambda}{d^{2/3}}e_r(\zeta),$$

where $e_r(\zeta)$ is a function of ζ. Hence, at fixed ζ, r is a monotonic decreasing function of d in region III: its maximum is attained at the boundary and is $\lambda 2^{-2/3}e_r(\zeta)$. Hence, as λ is small, the boundary-layer approximation is satisfied in region III.

We now consider regions I and II. In terms of $I_e(0;w,d)$ and $I_o(0;w,d)$, the inequality (4.13) is satisfied provided

$$\lambda|I_2| = \lambda\left|\frac{\partial^2 I_0}{\partial w^2}\right| \ll |I_0| \quad \text{for} \quad I_n = I_e(n;w,d)+\mathrm{i}I_o(n;w,d). \tag{4.19}$$

An extensive study of the ratio $R = |I_2/I_0|$ is given in Hurley & Keady (1996). The numerical calculations indicate that $R(w,d) < 200$ for $d > 1/16$ and all w; $R(w,d) < 200$ for $|w-1| > 1/16$ and all d. In the region away from d small and w near 1, 200 is much higher than needed, numbers less than eight being more appropriate. For given d, $s_+/a = d/\lambda$ which in the $(s_+/a, 1/\lambda)$-plane are straight lines through the origin. For all points on a particular line, the values of I_n will be the same. Hence the inequality (4.16) will be satisfied for λ sufficiently small. It is clear from the plots of the profiles of the inviscid solution that are given in Part 1 that the curvature of the profiles and hence $|I_2|$ increases as d decreases, so that the required value of λ for inequality (4.16) to be satisfied will decrease. However, it is also clear that, if we fix $s_+/a, 0 < s_+/a < \infty$, for λ sufficiently small (depending on s_+/a), inequality (4.16) will be satisfied.

However, the boundary-layer approximation is clearly not satisfied in the neighbourhoods of the points where the characteristics touch the cylinder. We now give some attention to this small region. Consider the point $\sigma_+/a = -1, s_+/a = 0$. Put $\sigma'_+ = \sigma_+/a, s'_+ = s_+/a$. On the halfline $s'_+ = 0, \sigma'_+ < -1$, ψ_+ has the inviscid values given in Part 1 so that $\partial\psi_+/\partial\sigma_+$ has an inverse square-root singularity at $s'_+ = 0, \sigma'_+ = -1$. Hence, if the boundary-layer approximation were valid, (2.9) would hold and $\partial\psi_+/\partial s_+$ would be more singular and hence of greater magnitude near the singular point. It follows that the appropriate approximation to (2.6) is the one which retains the highest derivatives, namely

$$\nabla^4\psi_+ = 0.$$

The solution of this equation which has the appropriate behaviour on $s'_+ = 0, \sigma'_+ < -1$ is

$$\psi_+ = 2^{1/2}\alpha_+ a r^{1/2}\sin(\tfrac{1}{2}\theta),$$

where the notation is $r = [(1+\sigma'_+)^2+(s'_+)^2]^{1/2}$ and θ is a polar angle. The preceding equation shows that ψ_+, and hence $\partial\psi_+/\partial\sigma'_+$, is even about the line $\theta = \pi$ and that both

https://doi.org/10.1017/S0022112097007039 Published online by Cambridge University Press

are continuous on it. Also $\partial\psi_+/\partial s'_+$ is odd about the line $\theta = 0$ and vanishes on it. It is also clear from (2.6) applied with ψ replaced by ψ_+ that the region in which it reduces to $\nabla^4\psi_+ = 0$ is of diameter order $\lambda^{1/2}$.

5. Comparison of results with those of other investigators

5.1. *The force exerted by the cylinder on the fluid*

Lighthill (1978, §4.10) considers a cylindrical wire oscillating horizontally and shows that in our notation

$$q = \frac{G\sin(\mu)}{4\pi N}\int_0^\infty k_0 \exp(-k_0^3\lambda s_+ + \mathrm{i}k_0\sigma_+)\,\mathrm{d}k_0, \tag{5.1}$$

where G is the force per unit length which the cylinder exerts on the fluid and q is the vertical component of the mass flux. Thus

$$q = \rho_0 \frac{\partial\psi_+}{\partial\sigma_+}\sin(\mu), \tag{5.2}$$

where ρ_0 is the density. Putting $K = k_0 a$, equation (5.1) gives

$$\frac{\partial\psi_+}{\partial\sigma_+} = \frac{G}{4\pi\rho_0 a^2 N}\int_0^\infty K\exp\left(-K^3\lambda\frac{s_+}{a} + \mathrm{i}K\frac{\sigma_+}{a}\right)\mathrm{d}K. \tag{5.3}$$

We recognize the integral in this equation as giving the similarity solution of Thomas & Stevenson (1972).

We interpret Lighthill's wire as being a circular cylinder of very small radius so that we compare his result with our asymptotic one given in (4.7). Using (3.7) and (3.5) with $V = 0$ gives

$$\frac{\partial\psi_+}{\partial\sigma_+} = \frac{U}{4}(\cos(\mu) - \mathrm{i}\sin(\mu))\int_0^\infty K\exp\left(-K^3\lambda\frac{s_+}{a} + \mathrm{i}K\frac{\sigma_+}{a}\right)\mathrm{d}K, \quad \lambda\frac{s_+}{a} \gg 1. \tag{5.4}$$

Comparison of (5.3) and (5.4) gives

$$G = \pi\rho_0 a^2 NU[\cos(\mu) - \mathrm{i}\sin(\mu)]. \tag{5.5}$$

It is interesting to compare this result with that given by the inviscid theory of Part 1. Equation (3.43) therein shows that the force per unit length that the cylinder exerts on the fluid is

$$-F_x = \pi\rho_0\omega a^2\eta U. \tag{5.6}$$

This result is expected to hold approximately for the viscous case when $\lambda \ll 1$, for then the discussion at the end of §4.4 suggests that the inviscid solution will be a good approximation everywhere on the surface of the cylinder except very near where the characteristics touch it. Equations (5.5) and (5.6) give

$$\frac{G}{-F_x} = [1 - \mathrm{i}\tan(\mu)]. \tag{5.7}$$

5.2. *The work of Makarov et al. (1990)*

We focus on this reference because it includes a comprehensive review of the theoretical and experimental work in Russia on a variety of problems involving internal waves. In model 4 of their paper they calculate the internal waves produced by a vibrating

https://doi.org/10.1017/S0022112097007039 Published online by Cambridge University Press

circular cylinder in a viscous fluid. Their equation (4) for the vertical desplacement h of the fluid particles is, in our notation,

$$h = -\tfrac{1}{2}\exp(-\mathrm{i}\omega t)\, a_0 \sin\mu \sin(\mu-\phi_0) \int_0^\infty J_1(K) \exp\left(\mathrm{i}K\frac{\sigma_+}{a} - K^3\lambda\frac{s_+}{a}\right)\mathrm{d}K, \tag{5.8}$$

where a_0 is the amplitude of the particle displacement and ϕ_0 is its inclination to the horizontal. The particle displacement h_{σ_+} in the direction of $\hat{\boldsymbol{\sigma}}_+$ (defined in figure 5 of Part 1) is $h/\sin\mu$ and differentiation with respect to t gives that the particle velocity in the direction of $\hat{\boldsymbol{\sigma}}_+$ is

$$\frac{\partial\psi_+^M}{\partial\sigma_+} = -\frac{\mathrm{i}}{2}\exp(-\mathrm{i}\omega t)\, a_0 w \sin(\mu-\phi_0) \int_0^\infty J_1(K) \exp\left(\mathrm{i}K\frac{\sigma_+}{a} - K^3\lambda\frac{s_+}{a}\right)\mathrm{d}K, \tag{5.9}$$

where the superscript M denotes Makarov *et al.* (1990). (Also, in (5.9), t is measured from $t_0 = -\pi/w$ to change the sign preceding its right-hand side.) Noting that

$$a_0 w \sin(\mu-\phi_0) = U\sin\mu - V\cos\mu, \tag{5.10}$$

(5.9) can be written

$$\frac{\partial\psi_+^M}{\partial\sigma_+} = -\frac{\mathrm{i}}{2}\exp(-\mathrm{i}\omega t)\,(U\sin\mu - V\cos\mu) \int_0^\infty J_1(K) \exp\left(\mathrm{i}K\frac{\sigma_+}{a} - K^3\lambda\frac{s_+}{a}\right)\mathrm{d}K. \tag{5.11}$$

The corresponding result in our solution with the time factor $\exp(-\mathrm{i}\omega t)$ added is

$$\frac{\partial\psi_+}{\partial\sigma_+} = -\frac{\mathrm{i}}{2}\exp(-\mathrm{i}\omega t)\,[U\sin\mu - V\cos\mu + \mathrm{i}(U\cos\mu + V\sin\mu)] \times \int_0^\infty J_1(K) \exp\left(\mathrm{i}K\frac{\sigma_+}{a} - K^3\lambda\frac{s_+}{a}\right)\mathrm{d}K. \tag{5.12}$$

We now compare our results with the experimental ones shown in their figure 3(*b*). For their experiments we find λ to be approximately 0.0019. Hence, using our figure 5, we find that the particle displacement on the centreline of the beam is approximately 0.61 mm which is in reasonable agreement with their experimental results. However, they state that their theoretical and experimental results differ by a factor of 6.5.

Finally, we consider results for the phase difference between the left- and right-hand beams versus the angle of inclination, $\ _0$, of the plane of oscillation to the horizontal. Their figure 2 shows excellent agreement between their theory and experiment. Our equations (3.3)–(3.6) give

$$\alpha_-/\alpha_+ = \exp(\mathrm{i}(\pi - 2\ _0)), \tag{5.13}$$

so that our results also agree with their experimental ones.

We can summarize the comparison of our results with those of Makarov *et al.* as follows. It is clear from (5.11) and (5.12) that both ψ_+^M and ψ_+ satisfy the same partial differential equation, namely (2.9). Also, (4.1), (4.2) and (4.8) of Part 1 make it clear that both $\psi_+ + \psi_-$ and $\psi_+^M + \psi_-^M$ satisfy the same (inviscid) boundary condition, namely (2.16). However, when the viscosity is taken to be zero ψ_+ reduces to the *exact* solution discussed in Part 1 but ψ_+^M does not and is therefore unsatisfactory.

https://doi.org/10.1017/S0022112097007039 Published online by Cambridge University Press

6. Application of results to a general elliptic cylinder

It is pointed out at the end of Appendix B that our approximate solution for general ellipses is given by

$$\psi_+ = \mp \mathrm{i}\alpha_+ c_+ \int_0^\infty \frac{J_1(K)}{K} \exp\left(\mp K^3 \lambda_+ \frac{s_+}{c_+} \pm \mathrm{i}K \frac{\sigma_+}{c_+} \right) \mathrm{d}K, \quad \pm s_+ > 0, \tag{6.1}$$

$$\psi_- = \pm \mathrm{i}\alpha_- c_- \int_0^\infty \frac{J_1(K)}{K} \exp\left(\mp K^3 \lambda_- \frac{s_-}{c_-} \mp \mathrm{i}K \frac{\sigma_-}{c_-} \right) \mathrm{d}K, \quad \pm s_- > 0 \tag{6.2}$$

on the understanding that the solution (6.1) for $s_+ > 0$ is continued up to the right-hand boundary of the ellipse shown in figure 8 (*b*) in Appendix B. Similarly the solution for $s_+ < 0$ is continued up to the left-hand boundary of the ellipse.

In (6.1) and (6.2) c_+, c_-, α_+ and α_+ are given by (3.14), (3.26) and (3.27) of Part 1. Also, λ_+ and λ_- are defined by

$$\lambda_+ = \frac{\nu}{2c_+^2 w\eta}, \quad \lambda_- = \frac{\nu}{2c_-^2 w\eta}, \tag{6.3}$$

see (3.1) herein.

Acknowledgements are gratefully given to the referees for helpful and constructive comments and for drawing our attention to several important references.

Appendix A. Derivation of equation (3.7)

A.1. *Fourier transforms in* σ

We focus on the beam of waves in the first quadrant.

Define

$$\sigma'_+ = \sigma_+/c_+ \quad \text{and} \quad s'_+ = s_+/c_+, \tag{A 1}$$

$$\ell_+(\psi_+) \equiv \frac{\partial^2 \psi_+}{\partial \sigma'_+ \partial s'_+} + \cot(2\mu) \frac{\partial^2 \psi_+}{\partial s'^2_+} + \mathrm{i}\lambda_+ \left(\frac{\partial^4 \psi_+}{\partial \sigma'^4_+} + 2 \frac{\partial^4 \psi_+}{\partial \sigma'^2_+ \partial s'^2_+} + \frac{\partial^4 \psi_+}{\partial s'^4_+} \right), \tag{A 2}$$

where λ_+ is defined in (6.3), and

$$\ell_{+,3}(\psi_+) \equiv \frac{\partial^2 \psi_+}{\partial \sigma_+ \partial s_+} + \mathrm{i}\lambda_+ \left(\frac{\partial^4 \psi_+}{\partial \sigma^4_+} \right). \tag{A 3}$$

In terms of these, (2.6) and (2.9) become respectively

$$\ell_+(\psi_+) = 0, \tag{A 4}$$

$$\ell_{+,3}(\psi_+) = 0, \tag{A 5}$$

both to be satisfied in the flow region. We always solve $\ell_+(\psi) = 0$ with boundary conditions that ψ and $\nabla\psi$ tend to zero at infinity. To save unnecessary writing, henceforth in this Appendix we drop the superscript prime (or equivalently take $c_+ = 1$).

Assume that the singularities of ψ are fairly mild so that we can define

$$\Psi_+(K) = \frac{1}{\sqrt{2\,\pi}} \int_{-\infty}^{\infty} \psi_+ \exp(-\mathrm{i}K\sigma_+)\, \mathrm{d}\sigma_+ \tag{A 6}$$

https://doi.org/10.1017/S0022112097007039 Published online by Cambridge University Press

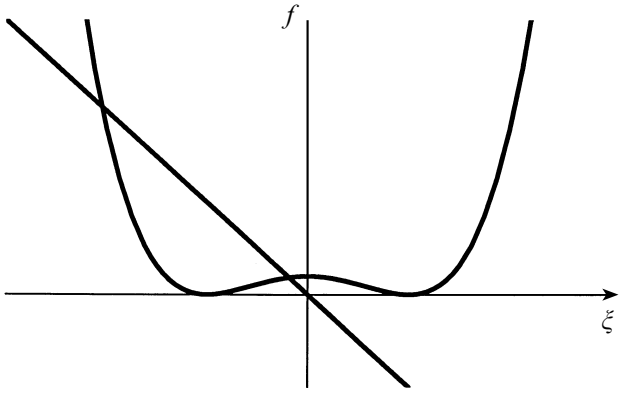


FIGURE 7. Roots of the quartic for $\mu = \pi/4$ (and $K > 0$). The line shown is $f = -\xi K/\lambda_+$: the quartic is $f = (\xi^2 - K^2)^2$. Their points of intersection, the real roots, are denoted ξ_j, $-K < \xi_2 < 0, \xi_3 < -K$.

as the Fourier transform of ψ_+, with inversion formula

$$\psi_+ = \frac{1}{\sqrt{2\pi}} \int_{-\infty}^{\infty} \Psi_+ \exp(\mathrm{i}K\sigma_+)\, \mathrm{d}K. \tag{A 7}$$

Taking a Fourier transform of $\ell_+(\psi_+) = 0$, see (A 2), gives

$$\frac{\mathrm{d}^4\Psi_+}{\mathrm{d}s_+^4} - \frac{\mathrm{d}^2\Psi_+}{\mathrm{d}s_+^2}\left(2K^2 + \frac{\mathrm{i}\cot(2\mu)}{\lambda_+}\right) + \frac{K}{\lambda_+}\frac{\mathrm{d}\Psi_+}{\mathrm{d}s_+} + K^4\Psi_+ = 0. \tag{A 8}$$

The equation

$$\Psi_+ = \Psi_{0,+}(K)\exp(\zeta s_+) \tag{A 9}$$

is a solution of (A 8) if

$$\zeta^4 - \zeta^2\left(2K^2 + \mathrm{i}\frac{\cot(2\mu)}{\lambda_+}\right) + \zeta\frac{K}{\lambda_+} + K^4 = 0. \tag{A 10}$$

Employing the method of the Principle of the Argument we find that the quartic polynomial (A 10) has (for $\mu \neq \pi/4$) one zero in each of the four quadrants of the $(\zeta = \xi + \mathrm{i}\eta)$-plane. We denote by ζ_i the zero in the ith quadrant.

When $K > 0$, the most general solution of (A 8) that decays for large positive s_+ is

$$\Psi_+ = c_2(K;\lambda_+)\exp(\zeta_2 s_+) + c_3(K;\lambda_+)\exp(\zeta_3 s_+). \tag{A 11}$$

A.2. *Roots of the quartic*, $\mu = \pi/4$

We temporarily consider $\mu = \pi/4$. Then (A 10) has one zero in each of the first and fourth quadrants and two on the negative ξ-axis and can be written

$$(\zeta^2 - K^2)^2 + \zeta K/\lambda_+ = 0, \tag{A 12}$$

so that the two zeros on the negative ξ-axis satisfy

$$(\xi^2 - K^2)^2 + \xi K/\lambda_+ = 0. \tag{A 13}$$

The location of the two real roots of (A 13), denoted by ξ_2 and ξ_3, are illustrated in figure 7.

We now examine ξ_3. Refer again to figure 7. We see that when $(K/\lambda_+) \gg 1$, $f = -K\xi/\lambda_+$ is nearly vertical, so that one root ξ_3 is large and negative,

$$\xi_3 \sim -(K/\lambda_+)^{1/3}, \quad K/\lambda_+ \to \infty,$$

https://doi.org/10.1017/S0022112097007039 Published online by Cambridge University Press

and the other real root ξ_2 is very nearly zero. This small root of (A 13) is approximated, at fixed $K > 0$, by

$$\xi_2 = -\lambda_+ K^3(1-2(\lambda_+ K^2)^2+9(\lambda_+ K^2)^4+\ldots) \quad \text{for} \quad \lambda_+ \to 0+. \tag{A 14}$$

Also, ξ_2 can be approximated, at fixed $\lambda_+ > 0$, by

$$\xi_2 \sim -K+\frac{1}{2\lambda_+^{1/2}}-\frac{1}{64K^2\lambda_+^{3/2}} \quad \text{for} \quad K \to +\infty.$$

On $s_+ = 0$, equation (A 11) gives $\Psi_+ = c_2(K)+c_3(K)$ so that

$$\psi_+ = \frac{1}{\sqrt{2\pi}}\int_{-\infty}^{\infty}(c_2(K)+c_3(K))\exp(\mathrm{i}K\sigma_+)\,\mathrm{d}K, \quad s_+ = 0. \tag{A 15}$$

On taking

$$(c_2(K)+c_3(K)) = -\mathrm{i}\sqrt{2\pi}\alpha_+ c_+ \frac{J_1(K)}{K}H(K), \tag{A 16}$$

where $H(K)$ denotes the Heaviside step function, which is 1 for $K > 0$ and 0 for $K < 0$, equation (A 11) and the inversion formula give ψ_+ that agree with the inviscid solution as s_+ tends to zero from above.

Now when λ_+ is small and $s_+ > 0$, the $c_3(K)$-term is negligible compared to the $c_2(K)$-term. This is established by the results of the preceding subsection concerning the roots of the quartic. From this, we obtain that, for $s_+ > 0$, we obtain correct asymptotics by replacing $c_2(K)$ by zero. Also, using the asymptotics of ξ_2 for λ_+ small, we see that we obtain correct asymptotics by replacing ξ_2 by $-\lambda_+ K^3$. This gives a derivation of (3.7).

A.3. *Return to the derivation of* (3.7)

We now return to the general case when $\mu \neq \pi/4$. Putting $\cot(2\mu) = \epsilon$, we find that the root equation (A 10) that reduces to $-\lambda_+ K^3$ as $\epsilon \to 0$ has a positive imaginary part and is in the second quadrant. Thus, again for λ_+ small, our proposed solution is

$$\psi_+ = -\mathrm{i}\alpha_+ c_+ \int_0^{\infty}\frac{J_1(K)}{K}\exp(\zeta_2 s'_+ + \mathrm{i}K\sigma'_+)\,\mathrm{d}K, \quad s'_+ \geqslant 0, \tag{A 17}$$

where ζ_2 is the root of equation (A 10) that lies in the second quadrant of the complex ζ-plane. When λ_+ is small, the quartic (A 10) is now approximated by

$$K^4+\zeta K/\lambda_+ = 0, \tag{A 18}$$

so that

$$\zeta = -\lambda_+ K^3, \tag{A 19}$$

and (A 17) becomes (3.7).

However, (A 17) has one major defect, because it may readily be shown that it gives values of $\partial\psi_+/\partial s_+$ which are not continuous on $s_+ = 0, |\sigma_+| > 1$. However, (3.7) does not have this defect, as was shown in §3.1 of the main text.

We note that ψ_+ given by (3.7) satisfies (A 5) exactly but (A 4) only approximately.

Appendix B. Representation of the solution by distributions of semi-vortices

We are concerned with developing a representation of our solution by a distribution of singular solutions in the case $\lambda \ll 1$ when the viscous solution tends to the inviscid one close to the cylinder. The first step is to find such a representation for the inviscid solution given by (3.35)–(3.37) of Part 1.

https://doi.org/10.1017/S0022112097007039 Published online by Cambridge University Press

B.1. *The inviscid case*

Makarov *et al.* (1990) expressed their solution in terms of a distribution of dipoles. We prefer to use vortices.

The solution for a point vortex in a stratified fluid was given by Robinson (1969) for the case when the fluid was confined above and below by two horizontal plane walls. The solution was adapted by Hurley (1969) to the case of an unbounded fluid. Thus in accordance with his equation (3.18) we take as the singular solution

$$\begin{aligned}\psi_V &= (1/\pi)\log(\sigma_+\,\sigma_-)\\ &= \mathrm{i}[2-H(\sigma_+)-H(\sigma_-)]+(1/\pi)\log|\sigma_+\,\sigma_-|, \quad x>0,\end{aligned} \tag{B 1}$$

and ψ_V is defined to be an even function of x.

We express

$$\left.\begin{aligned}\psi_V &= \psi_{V+}+\psi_{V-},\\ \text{where}\quad \psi_{V+}(\sigma_+) &= (1/\pi)\log\sigma_+\\ \text{and}\quad \psi_{V-}(\sigma_-) &= (1/\pi)\log\sigma_-;\end{aligned}\right\} \tag{B 2}$$

ψ_{V+} and ψ_{V-} will be referred to as 'semi-vortices' because their sum is a vortex. The Green's function for the antisymmetric motion of a flat plate was shown in Hurley (1969) to be, in our notation, proportional to

$$g(s') = \frac{s'}{(1-s'^2)^{1/2}}, \tag{B 3}$$

where $s'=s/a$ and s is the distance of a point on the plate from its centre, the length of the plate being $2a$. Define $\sigma'_+=\sigma_+/a$, $\sigma'_-=\sigma_-/a$, $\tau'_+=\tau_+/a$, $\tau'_-=\tau_-/a$. We now show that the solutions for a circular cylinder can be expressed as

$$\left.\begin{aligned}\psi_+ &= \frac{\alpha_+ a}{\pi}\int_{\Gamma_+}\frac{\tau'_+\log(\tau'_+-\sigma'_+)}{(1-\tau'^2_+)^{1/2}}\,\mathrm{d}\tau'_+,\\ \psi_- &= \frac{\alpha_- a}{\pi}\int_{\Gamma_-}\frac{\tau'_-\log(\tau'_--\sigma'_-)}{(1-\tau'^2_-)^{1/2}}\,\mathrm{d}\tau'_-,\end{aligned}\right\} \tag{B 4}$$

where Γ_+ and Γ_- are the interval $(-1,1)$ of the $O\tau'_+$ and $O\tau'_-$ axes shown in figure 8(*a*). Γ_+ is indented below $\tau_+=\sigma_+$ for $s_+>0$ and above it for $s_+<0$.

Differentiation of the first of (B 4) gives

$$\begin{aligned}\frac{\partial\psi_+}{\partial\sigma_+} &= \pm\frac{\mathrm{i}\alpha_+\,\sigma'_+}{(1-\sigma'^2_+)^{1/2}}+\frac{\alpha_+}{\pi}\mathscr{P}\int_{-1}^{1}\frac{\tau'_+\,\mathrm{d}\tau'_+}{(1-\tau'^2_+)^{1/2}(\tau'_+-\sigma'_+)}, \quad |\sigma'_+|<1,\\ &= \frac{\alpha_+}{\pi}\int_{-1}^{1}\frac{\tau'_+\,\mathrm{d}\tau'_+}{(1-\tau'^2_+)^{1/2}(\tau'_+-\sigma'_+)}, \quad |\sigma_+|>1,\end{aligned}$$

where $\mathscr{P}$ denotes the Cauchy principal value, and where in the first equation the upper sign is for $s_+>0$ and the lower sign for $s_+<0$.

Using the results

$$\mathscr{P}\int_{-1}^{1}\frac{\tau'_+\,\mathrm{d}\tau'_+}{(1-\tau'^2_+)^{1/2}(\tau'_+-\sigma'_+)}=\pi,$$

https://doi.org/10.1017/S0022112097007039 Published online by Cambridge University Press

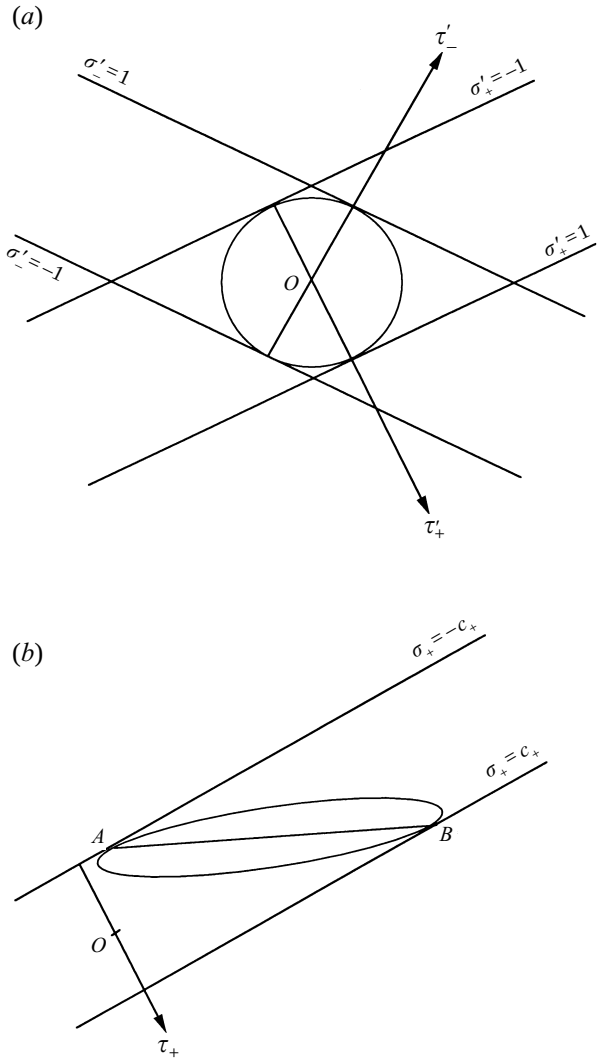


FIGURE 8. Location of semi-vortices for (*a*) circular cylinders, (*b*) elliptic cylinders.

and
$$\int_{-1}^{1} \frac{\tau'_+ \,\mathrm{d}\tau'_+}{(1-\tau'^2_+)^{1/2}(\tau'_+ - \sigma'_+)} = 1 + \begin{cases} \dfrac{-\sigma'_+}{(\sigma'^2_+ - 1)^{1/2}} & \text{for} \quad \sigma'_+ > 1 \\ \dfrac{+\sigma'_+}{(\sigma'^2_+ - 1)^{1/2}} & \text{for} \quad \sigma'_+ < -1, \end{cases}$$

we find that $\partial\psi_+/\partial\sigma_+$ takes the values given by (3.30) of Part 1 as desired.

B.2. *The viscous case*

Equations (B 2) and (B 4) show that the inviscid solution for ψ_+ can be expressed as

$$\psi_+ = \alpha_+ a \int_{\Gamma_+} \frac{\tau'_+ \psi_{V+}(\tau'_+ - \sigma'_+)\,\mathrm{d}\tau'_+}{(1-\tau'^2_+)^{1/2}}, \tag{B 5}$$

where $\psi_{V+}(\sigma_+)$ is given by (B 2).

https://doi.org/10.1017/S0022112097007039 Published online by Cambridge University Press

Now it can be shown that ψ_{V+} is the solution, having appropriate behaviour at large distances, of the equation

$$\eta^2 \frac{\partial^2 \psi_{V+}}{\partial x'^2} - \frac{\partial^2 \psi_{V+}}{\partial y'^2} = -2\mathrm{i}\delta(x')\,\delta(y'). \tag{B 6}$$

Thus referring to equation (2.2) of the main text and (B 5) and (B 6) above we take as the viscous solution

$$\psi_+^v = \alpha_+ a \int_{\Gamma_+} \frac{\tau'_+ \psi_{V+}^v(\tau'_+ - \sigma'_+)\,\mathrm{d}\tau'_+}{(1-\tau'^2_+)^{1/2}}, \tag{B 7}$$

where ψ_{V+}^v satisfies

$$\eta^2 \frac{\partial^2 \psi_{V+}^v}{\partial x'^2} - \frac{\partial^2 \psi_{V+}^v}{\partial y'^2} + \mathrm{i}\lambda\nabla^4 \psi_{V+}^v = -2\mathrm{i}\delta(x')\,\delta(y'). \tag{B 8}$$

The solution of (B 8) clearly tends to that of (B 6) as λ tends to zero. Using (2.6) we see that referred to the (σ'_+, s'_+) axes (B 8) is

$$\frac{\partial^2 \psi_{V+}^v}{\partial \sigma'_+ \partial s'_+} + \cot(2\mu)\frac{\partial^2 \psi_{V+}^v}{\partial s'^2_+} + \mathrm{i}\lambda\nabla^4 \psi_{V+}^v = -2\mathrm{i}\delta(\sigma'_+)\,\delta(s'_+). \tag{B 9}$$

Let

$$\bar{\psi}_{V+}^v = \frac{1}{2\pi}\int_{-\infty}^{\infty}\int_{-\infty}^{\infty} \psi_{V+}^v \exp(-\mathrm{i}K\sigma'_+ - \mathrm{i}ks'_+)\,\mathrm{d}\sigma'_+\,\mathrm{d}s'_+,$$

so that by (B 9)

$$\bar{\psi}_{V+}^v = \frac{-\mathrm{i}}{\pi(-kK - k^2\cot(2\mu) + \mathrm{i}\lambda(K^4 + 2K^2k^2 + k^4)}.$$

This gives

$$\psi_{V+}^v = \frac{-\mathrm{i}}{2\pi^2}\int_{-\infty}^{\infty}\int_0^{\infty} \frac{\exp(+\mathrm{i}K\sigma'_+ + \mathrm{i}ks'_+)\,\mathrm{d}K\,\mathrm{d}k}{-kK - k^2\cot(2\mu) + \mathrm{i}\lambda(K^2+k^2)^2}, \tag{B 10}$$

where only those waves having positive values of K are included so that the radiation condition is satisfied.

We carry out the integration with respect to k first. Let $D(k) = -kK - k^2\cot(2\mu) + \mathrm{i}\lambda(K^2+k^2)^2$, so that

$$D(-\mathrm{i}\zeta) = \mathrm{i}\lambda[\zeta^4 + \zeta^2(2K^2 + \mathrm{i}\cot(2\mu)/\lambda) + K\zeta/\lambda + K^4]. \tag{B 11}$$

We note that the above polynomial in ζ is the same as the left-hand side of (A 10). This polynomial has roots at ζ_i, $i = 1, 2, 3, 4$. The corresponding zeros of $D(k)$ are $k_i = -\mathrm{i}\zeta_i$. We find that k_2 and k_3 are in the upper half-plane and k_1 and k_4 are in the lower half-plane. It was shown in Appendix A that in the limit $\lambda \to 0$ the contribution from ζ_2 was dominant. Hence

$$\begin{aligned}\psi_{V+}^v &\sim \frac{-1}{\pi}\int_0^{\infty} \frac{\exp(+\mathrm{i}K\sigma'_+ + \zeta_2 s'_+)}{K}\,\mathrm{d}K, \quad s_+ > 0, \lambda \to 0 \\ &\sim \frac{-1}{\pi}\int_0^{\infty} \frac{\exp(+\mathrm{i}K\sigma'_+ - \lambda K^3 s'_+)}{K}\,\mathrm{d}K,\end{aligned} \tag{B 12}$$

using (A 14). Substitution into (B 7) gives

$$\psi_+^v = \frac{-\alpha_+ a}{\pi}\int_0^{\infty} \frac{\exp(-\mathrm{i}K\sigma'_+ - \lambda K^3 s'_+)}{K} I(K)\,\mathrm{d}K, \quad s_+ > 0, \tag{B 13}$$

https://doi.org/10.1017/S0022112097007039 Published online by Cambridge University Press

where

$$I(K) = \int_{-1}^{1} \frac{\tau'_+}{(1-\tau'^2_+)^{1/2}} \exp(\mathrm{i}K\tau'_+)\,\mathrm{d}\tau'_+.$$

Noting that

$$\int_{-1}^{1} \frac{\tau'_+ \exp(\mathrm{i}K\sigma'_+)\,\mathrm{d}\tau'_+}{(1-\tau'^2_+)^{1/2}} = \mathrm{i}\pi J_1(K),$$

equation (B 13) gives

$$\psi^v_+ = -\mathrm{i}\alpha_+ a \int_0^\infty \frac{J_1(K)}{K} \exp(\mathrm{i}K\sigma'_+ - \lambda K^3 s'_+)\,\mathrm{d}K,$$

in agreement with (3.3) of the main text.

We now consider the problem for the general ellipse shown in figure 8(*b*), where AB is the straight line joining the points where the ellipse touches the characteristics $\sigma_+ = \pm c_+$.

It is clear from the discussion in §3.2 that the viscous solution given by (B 7) (with α_+ having the appropriate value given by (3.26) of Part 1) will approximate the inviscid solution on the portion of the ellipse to the right of the line AB with arbitrarily small relative error with λ sufficiently small provided that the $O\tau_+$-axis is taken to be to the left of AB. The solution to the left of AB may similarly be constructed if the $O\tau_+$-axis is taken to be to the right of AB. Hence we can replace (3.3) by

$$\psi_+ = \mp \mathrm{i}\alpha_+ c_+ \int_0^\infty \frac{J_1(K)}{K} \exp(\mp K^3\lambda_+ s_+/c_+ \pm \mathrm{i}K\sigma'_+/c_+)\,\mathrm{d}K, \quad \pm s_+ > 0 \qquad \text{(B 13)}$$

on the understanding that the solution for $s_+ > 0$ is continued up to the right-hand boundary of the ellipse shown in figure 8(*b*). Similarly for $+s_+ < 0$.

In (B 13) c_+ and α_+ are given by (3.14) and (3.26) of Part 1 and

$$\lambda_+ = \frac{\nu}{2\chi_+^2\,\omega\eta}, \qquad \text{(B 14)}$$

see (3.1) herein.

REFERENCES

Batchelor, G. K. 1967 *An Introduction to Fluid Dynamics*. Cambridge University Press.

Bell, T. H. 1975 Lee waves in stratified flows with simple harmonic time dependence. *J. Fluid Mech.* **67**, 703–722.

Hurley, D. G. 1969 The emission of internal waves by vibrating cylinders. *J. Fluid Mech.* **36**, 657–672.

Hurley, D. G. 1997 The generation of internal waves by vibrating elliptic cylinders. Part 1. Inviscid solution. *J. Fluid Mech.* **351**, 105–118.

Hurley, D. G. & Keady, G. 1996 The generation of internal waves by vibrating cylinders. Part II. Approximate viscous solution for a circular cylinder. *Res. Rep., Dept. of Mathematics, University of Western Australia.*

Ivanov, A. V. 1989 Generation of internal waves by an oscillating source. *Izv. Atmos. Ocean. Phys.* **25**, 61–64.

Lighthill, J. 1978 *Waves in Fluids*. Cambridge University Press.

Makarov, S. A., Neklyudov, V. I. & Chasheckin, Yu. D. 1990 Spatial structure of two-dimensional monochromatic internal-wave beams in an exponentially stratified liquid. *Izv. Atmos. Ocean. Phys.* **26**, 548–554.

Robinson, R. M. 1969 The effect of a vertical barrier on internal waves. *Deep-Sea Res.* **16**, 421–429.

Rosenhead, L. 1963 *Laminar Boundary Layers*. Oxford University Press.

Thomas, N. H. & Stevenson, T. N. 1972 A similarity solution of viscous internal waves. *J. Fluid Mech.* **54**, 495–506.

Townsend, A. A. 1966 Internal waves produced by a convective layer. *J. Fluid Mech.* **24**, 307–319.

https://doi.org/10.1017/S0022112097007039 Published online by Cambridge University Press